Geophysical Journal International

Geophys. J. Int. (2016) **204,** 1159–1163 doi: 10.1093/gji/ggv501
GJI Seismology

EXPRESS LETTER

Statistical redundancy of instantaneous phases: theory and application to the seismic ambient wavefield

I. Gaudot,[1] É. Beucler,[1] A. Mocquet,[1] M. Schimmel[2] and M. Le Feuvre[3]

[1] *Laboratoire de Planétologie et de Géodynamique, Nantes University, UMR-CNRS* 6112, BP92208 F-44322 *Nantes, France.*
E-mail: ianis.gaudot@univ-nantes.fr
[2] *Institute of Earth Sciences Jaume Almera, CSIC, Lluis Sole i Sabaris s/n,* E-08028 *Barcelona, Spain*
[3] *IFSTTAR, Laboratory for Geophysics and Non Destructive Evaluation, LUNAM University,* CS4 F-44344 *Bouguenais, France*

Accepted 2015 November 16. Received 2015 November 10; in original form 2015 August 28

SUMMARY

In order to detect possible signal redundancies in the ambient seismic wavefield, we develop a new method based on pairwise comparisons among a set of synchronous time-series. This approach is based on instantaneous phase coherence statistics. The first and second moments of the pairwise phase coherence distribution are used to characterize the phase randomness. For perfect phase randomness, the theoretical values of the mean and variance are equal to 0 and $\sqrt{1-2/\pi}$, respectively. As a consequence, any deviation from these values indicates the presence of a redundant phase in the raw continuous signal. A previously detected microseismic source in the Gulf of Guinea is used to illustrate one of the possible ways of handling phase coherence statistics. The proposed approach allows us to properly localize this persistent source, and to quantify its contribution to the overall seismic ambient wavefield. The strength of the phase coherence statistics relies in its ability to quantify the redundancy of a given phase among a set of time-series with various useful applications in seismic noise-based studies (tomography and/or source characterization).

Key words: Time-series analysis; Interferometry; Theoretical seismology; Statistical seismology; Wave propagation; Africa.

1 INTRODUCTION

The seismic ambient wavefield encompasses all possible displacements of the Earth's surface that are recordable by a seismometer. Since the beginning of the 20th century, the main goal of seismic station deployments is the analysis of transient signals caused by impulsive sources such as earthquakes or artificial sources, relegating the remaining signal (outside of the time window of interest) to seismic noise. The term 'noise' hence refers to anything else that modifies, perturbs, or hides the signal of interest. It is mostly generated in different frequency bands, such as the short-period (<1 s) anthropogenic noise (Koper *et al.* 2010), the 1–20 s period microseismic energy due to the ocean activity (e.g. Longuet-Higgins 1950; Gerstoft *et al.* 2008; Ebeling 2012) or oceanic long-period (>50 s) infragravity waves (Kobayashi & Nishida 1998; Rhie & Romanowicz 2004). However, the theoretical result that the cross-correlation of continuous noise converges toward the Green's function between two stations (e.g. Lobkis & Weaver 2001) has opened a variety of applications in seismology for retrieving information about the Earth's structure (e.g. Shapiro *et al.* 2005; Brenguier *et al.* 2008).

The empirical Green's function builds up after a sufficient self-averaging process which is provided by a random/uniform spatial distribution of the noise sources over time as well as scattering (Campillo 2006). Hence, high energetic signals due to short transient events can contaminate the cross-correlation results. Long time-averaged cross-correlations are also widely used to study the continuous excitation of the seismic ambient wavefield (e.g. Stehly *et al.* 2006). Amplitude normalization processing schemes are usually applied on raw time-series in order to wipe out the effects due to high amplitude transients events (such as earthquakes) (Bensen *et al.* 2007). The main drawback of these approaches is that normalizations corrupt the genuine signal information. Groos *et al.* (2012) pointed out that such normalization may lead to an amplification of signals generated by temporally persistent and spatially localized sources (e.g. Oliver 1962; Zeng & Ni 2010; Tonegawa *et al.* 2015). Moreover, amplitude normalization tends to favour distant sources compared to local contributions (Tian & Ritzwoller 2015).

The aim of this paper is to present a new method to provide quantitative information on the seismic ambient wavefield from the raw signal. The technique relies on phase repetitiveness of cross-correlations, and is based on the statistics of a time sample-based pairwise comparison of instantaneous phase coherence. Instantaneous phases have been used in the field of communication (Gabor 1946), medecine (Mormann *et al.* 2000), seismic exploration (Taner

et al. 1979) and for seismic signal extraction (Schimmel & Paulssen 1997).

2 COHERENCE STATISTICS

2.1 Theory

In the complex trace analysis framework, any sample of a signal can be defined in the complex plane as an instantaneous vector with length $A(t)$ and direction angle $\phi(t)$, corresponding to the envelope and the instantaneous phase, respectively (Gabor 1946; Taner *et al.* 1979). The analytic signal S is computed using $\mathcal{H}$, the Hilbert transform of the real input signal s,

$$S(t) = s(t) + i\mathcal{H}(t) = A(t)\exp[i\phi(t)]. \tag{1}$$

At a given time, instantaneous phases can be used as a measurement of the (in)coherence among a set of traces (Schimmel & Paulssen 1997). The so-called phase stack, relies on constructive and destructive sums of unit vectors in the complex plane. In the case of only two signals, s_j and s_k, the phase coherence (Schimmel 1999), at a given time t,

$$c_{jk}(t) = \frac{1}{2}\left|e^{i\phi_j(t)} + e^{i\phi_k(t)}\right| - \frac{1}{2}\left|e^{i\phi_j(t)} - e^{i\phi_k(t)}\right|, \tag{2}$$

is a real value lying between -1 and 1. Thus, a coherence value of 1 is obtained for a perfect phase match, and conversely for -1. Defining $\delta\phi_{jk}(t) \equiv \phi_k(t) - \phi_j(t)$, where $\delta\phi_{jk}(t) \in [-\pi, \pi]$,

$$c_{jk}(t) = \left|\cos\frac{\delta\phi_{jk}(t)}{2}\right| - \left|\sin\frac{\delta\phi_{jk}(t)}{2}\right|. \tag{3}$$

With the aim of introducing statistical quantities to compare a set of n synchronous signals, we define $\mu_j(t)$, the mean of coherences between the jth and all other instantaneous phases (hereafter referred to as individual coherences),

$$\mu_j(t) = \frac{1}{n-1}\sum_{k=1}^{n}(1-\delta_{jk})c_{jk}(t), \tag{4}$$

where δ is the Kronecker symbol. A comprehensive pairwise comparison is obtained through the overall coherence,

$$\bar{\mu}(t) = \frac{1}{n}\sum_{j=1}^{n}\mu_j(t). \tag{5}$$

Since $c_{jk} = c_{kj}$ (eq. 2), all pairwise coherence values, stored in an $[n \times n]$ array (discarding the diagonal elements), are reshaped into a set C of p elements, where $p = n(n-1)/2$ and $C_i \equiv (c_{jk} + c_{kj})/2$. This leads to another definition of the overall coherence,

$$\bar{\mu}(t) = \frac{1}{p}\sum_{i=1}^{p}C_i(t). \tag{6}$$

The standard deviation $\bar{\sigma}$ is given by the variance,

$$\bar{\sigma}^2(t) = \frac{1}{p}\sum_{i=1}^{p}(C_i(t) - \bar{\mu}(t))^2. \tag{7}$$

To quantify the instantaneous phase redundancy, we first consider the case of random signals. A uniform distribution of instantaneous phases is a property of such signals (White 1991). According to the ergodicity property of randomness, the phase distribution at a given time is uniform among a set of n independently generated random signals. As a consequence, since the instantaneous phase differences are computed for all $\phi_k(t)$ while keeping $\phi_j(t)$ fixed, $\delta\phi_{jk}(t)$ is uniformly distributed as well.

Considering that, for a sufficient large amount of randomly distributed instantaneous phase differences, a random exploration of $[-\pi, \pi]$ is analogous to a regularly spaced sampling of that domain. Introducing x as any instantaneous phase shift measurement $\delta\phi_{jk}(t)$, the mean value $\bar{\mu}$ of the coherences $C(x)$ may be equivalently defined in its continuous form or using the first moment definition,

$$\frac{1}{2\pi}\int_{-\pi}^{\pi}C(x)\,dx = \int_{-1}^{1}C\mathcal{P}(C)\,dC, \tag{8}$$

where $\mathcal{P}(C)$ is a probability density function. Eq. (8) with the phase coherence definition (eq. 3) leads to

$$\mathcal{P}(C) = \frac{2}{\pi\sqrt{2-C^2}} \quad \text{and} \quad \bar{\mu} = 0. \tag{9}$$

Using the second moment definition and eq. (7), $\bar{\sigma}^2 = 1 - 2/\pi$. As shown in Fig. 1, the results for a regular sampling of $\delta\phi_{jk}$, between $-\pi$ and $+\pi$, perfectly match the theoretical predictions (eq. 9). The probability density function $\mathcal{P}(C)$ also predicts the behaviour of the distribution for the random case (green bars). The results are shown here for a set of $n = 300$ randomly distributed samples ($p = 44\,850$ comparisons). All experiments confirm that the uniform instantaneous phase distribution favours phase and antiphase coherences (C close to ± 1).

2.2 Synthetic experiment

To illustrate both cases of instantaneous phase randomness and redundancy, we present a synthetic experiment which mimics a temporally persistent signal within a background noise. A single noisy 120 000 s long time-series is constructed by sampling an amplitude value within a Gaussian distribution ($\mu = 0$, $\sigma = 0.22$) for each time sample. Starting at 200 s, 270 cosine tapered monochromatic signals of 100 s length and 20 s period, are added every 400 s. We then cut the time-series every 400 s to create a set of 300 data segments. As a result, the overprinted monochromatic signal is present within the 200–300 s time windows on each trace (between the two vertical lines in Fig. 2a), except for 30 traces (for instance, the red trace).

At each time, both individual and overall coherences are computed using eqs (4) and (6), respectively (Fig. 2b). In agreement with theoretical expectations (eq. 9), $\bar{\mu}$ statistically converges toward zero, and $\bar{\sigma}$ tends to a value of $\sqrt{1-2/\pi}(\simeq 0.603)$, for all time samples but those between 200 and 300 s. The limited amount of comparisons ($p = 44\,850$) is however sufficient to fit the random case theory, which emphasizes that the overall coherence statistically converges toward the expected value although the distribution of coherences, for such a limited amount of samples, does not perfectly fit the theoretical distribution (Fig. 1). The phase redundancy of the sinusoidal signals between 200 and 300 s significantly increases the $\bar{\mu}$ values up to 0.69. This latter value corresponds to an average of 270 individual coherences of approximately 0.85 among 300, since the 30 sums of individual coherences for pure random noise traces tend to zero. Two individual coherences (eq. 4) using only 299 comparisons are also computed (Fig. 2b). The differences between theory and synthetics for the random cases (outside the 200–300 s time window) are consequently larger than for $\bar{\mu}$ although a fairly good agreement is still achieved (values for the random case do not exceed 0.08). The polar grey-shaded density plots exhibit the distribution of instantaneous phases at two given time samples. They are both computed using the 299 instantaneous

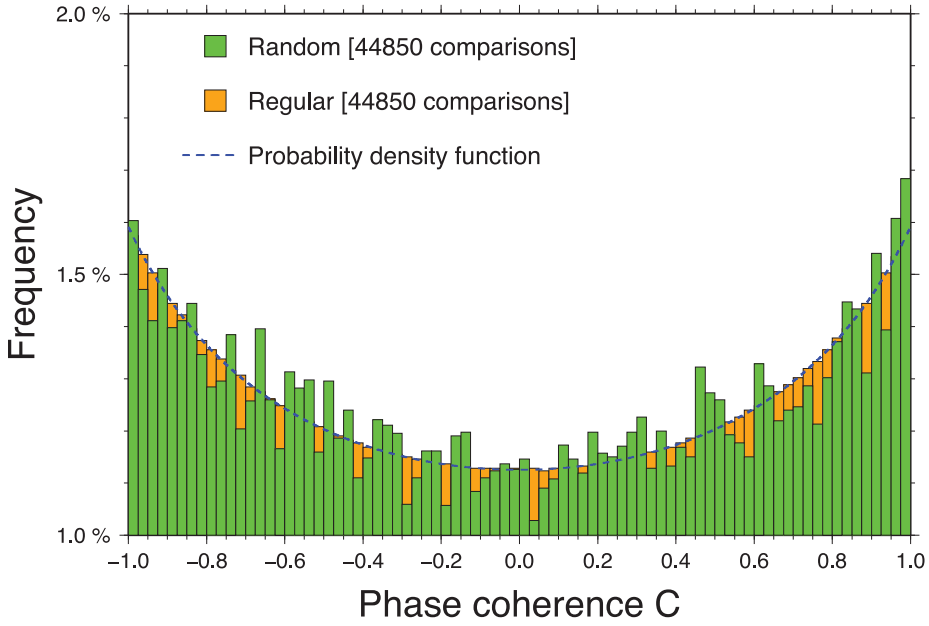

Figure 1. Comparison between theoretical predictions and numerical experiment results using $n = 300$ samples (i.e. $p = 44\,850$). The theoretical probability density function $\mathcal{P}(C)$ (eq. 9) is plotted with the dashed blue curve. The histogram obtained for a random sampling of $\delta\phi_{jk}$ (green) overlays the results obtained using a regular sampling (orange).

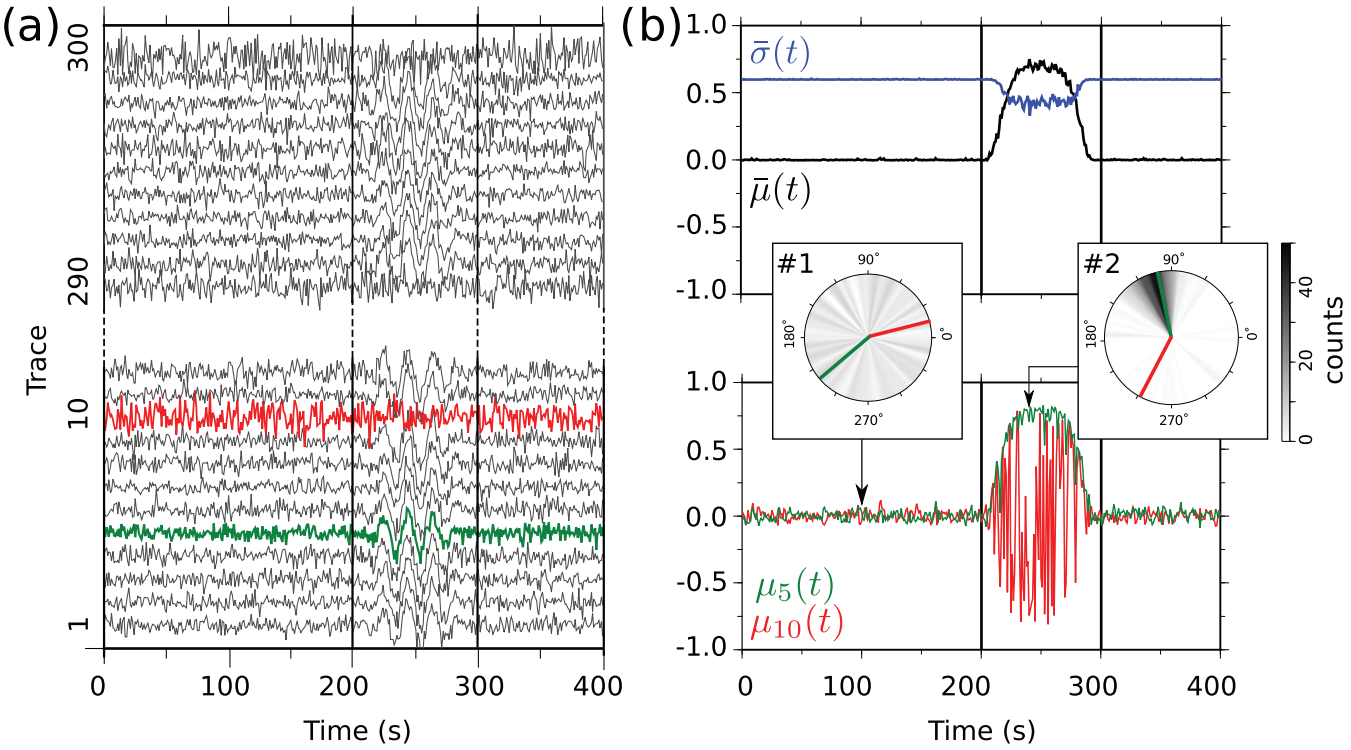

Figure 2. Statistics results using synthetic time-series. (a) Set of 300 time-series showing the presence of the sine signal added for 90 per cent of the traces, between 200 and 300 s. All time-series are carried by a random Gaussian noise. The red and green traces are used as reference for individual coherences in the lower right graph. (b) Top: overall coherence (black) and standard deviation (blue) computed using 44 850 pairwise comparisons. Bottom: individual coherences for traces 5 (green) and 10 (red), and instantaneous phase density plots in the complex plane, at $t = 100$ s (middle panel 1) and $t = 240$ s (middle panel 2). For each density plot, the instantaneous phases for traces 5 and 10 are plotted.

phase values. At $t = 100$ s (panel 1), the almost uniform density is a consequence of the random case, while at $t = 240$ s (panel 2), the phase redundancy results in the concentration of the density within a narrow angular range. The instantaneous phases ϕ_5 and ϕ_{10}, used as references for individual coherence measurements (eq. 4), overlay the density plots in green and red colours, respectively. At $t = 100$ s, their exact values have no impact on μ_5 and μ_{10} due to the uniform density. Conversely, at $t = 240$ s, the values of instantaneous phases ϕ_5 and ϕ_{10} greatly influence the individual statistics results. As shown in Fig. 2(a), the 5th time-series (green) contains the sine

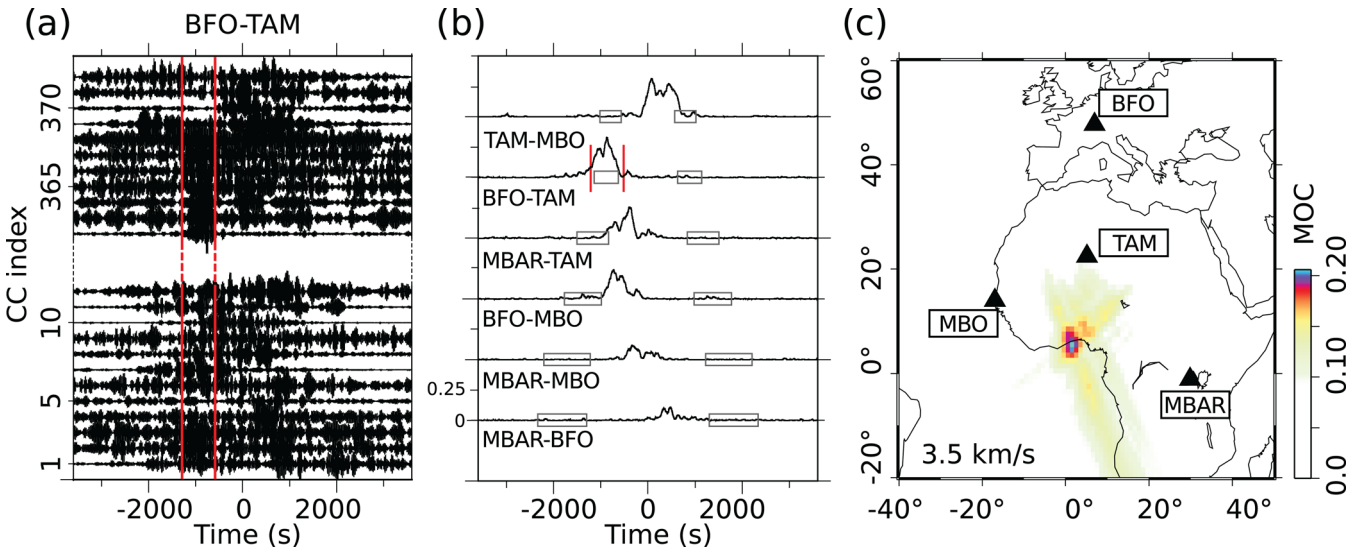

Figure 3. Location of the 26 s period persistent microseismic source using overall coherences on ambient seismic cross-correlations. (a) Subset of the 372 cross-correlations computed for the BFO-TAM station pair. The vertical red bars indicate the time window of large overall coherence values detected and shown in (b). Data are bandpass filtered between 23 and 32 s period. (b) Overall coherences for the six station pairs. The grey boxes define the time windows that would be expected for the propagation of a surface wave along the interstation great-circle paths using classical group velocity values (2.5 km $s^{-1} \leq U \leq 4.5$ km s^{-1}). (c) Source location using eqs. (10) and (11). Seismic stations are represented by the black triangles. Each time sample, and its corresponding mean coherence value (see (b)), is projected on the grid using an homogeneous velocity set to 3.5 km s^{-1}.

signal leading to a value for ϕ_5 close to the density maximum. As a consequence, for all time samples within 200 and 300 s, μ_5 is positive and much larger than zero, which signs a departure from the previously discussed random case. Low or negative values of individual coherences (such as μ_{10} at $t = 240$ s, for instance) are representative of a large difference between ϕ_{10} (red in panel 2) and the maximum of the instantaneous phase density. The overall randomness of the 10th time-series (red) implies large variations of the individual coherences as a function of time, though high values for μ_{10} can be reached but only by chance.

3 APPLICATION TO THE MICROSEISMIC SOURCE IN THE GULF OF GUINEA

Temporally persistent and spatially localized microseismic sources have been detected at different places around the world (e.g. Holcomb 1980). Some of them have been localized using ambient noise cross-correlations (e.g. Shapiro *et al.* 2006; Brzak *et al.* 2009; Zeng & Ni 2010; Xia *et al.* 2013). We propose to focus on the 26 s period source located near the Gulf of Guinea, using a sparse seismic array composed of four broad-band Federation of Digital Seismograph Network stations. The initial set of observations consists in continuous vertical component data, recorded during the month of 2004 August (Shapiro *et al.* 2006).

To compute coherence statistics among a set composed of a sufficient number of synchronous traces, the raw seismic signal is split into 372 2-hr sliding time windows. Only the basic signal processing steps (including removing the mean, trend and the instrumental response) are applied. Data are bandpass filtered between 23 and 32 s periods. The 2-hr time-series are cross-correlated, leading to a set of 372 synchronous cross-correlations for each station pair (Fig. 3a). The overall coherence measurements (eq. 5) are computed for each station pair (Fig. 3b). For all station pairs, the overall coherence $\bar{\mu}(t)$ value is close to zero for most time lags except for specific time windows in which a clear signal emerges. A fairly simple approach is followed to convert mean overall coherences into geographical locations. We test any possible source position using a grid of 80° × 90°, every 1°.

$$\tau_{ij}(\lambda, \Phi) = \frac{\Delta_i(\lambda_i, \Phi_i, \lambda, \Phi) - \Delta_j(\lambda_j, \Phi_j, \lambda, \Phi)}{U}, \quad (10)$$

is the traveltime delay between a given gridpoint (located at latitude λ and longitude Φ) and a given station pair. The epicentral distances (Δ_i and Δ_j) between the two stations (i and j) and the gridpoint are computed on a spherical Earth. Following Shapiro *et al.* (2006), a homogeneous surface wave group velocity $U = 3.5$ km s^{-1} is chosen.

For each gridpoint, the mean overall coherence

$$\mathrm{MOC}(\lambda, \Phi) = \frac{2}{n(n-1)} \sum_{i=1}^{n-1} \sum_{j=i+1}^{n} \bar{\mu}_{ij}(\tau_{ij}), \quad (11)$$

is computed (Fig. 3c), n is the amount of stations ($n = 4$). The maximum amplitude is at (5.5°N, 1.5°E), which is in very good agreement with previous locations found in the literature (Shapiro *et al.* 2006; Xia *et al.* 2013). The smearing features are due to the very small amount of stations.

The study of microseism sources from ambient noise cross-correlations usually requires pre-cross-correlation time normalization in order to attenuate the effects due to the presence of large amplitude events (Shapiro *et al.* 2006). Here, no time normalization and no spectral whitening is applied, since only the information carried by the instantaneous phases is used. Although most of the 2-hr-cross-correlations are very noisy (Fig. 3a), the pairwise statistics on phase coherences give very robust features and quantify the signal randomness (values around zero) as well as the phase redundancy. The overall coherence results (Fig. 3b) show that it is possible to quantify the weight of a repetitive source in the seismic ambient wavefield. The statistics confirm that the Gulf of Guinea source is redundant within the 23–32 s period range. However, the largest overall coherences values are significantly lower than 1 (0.33 for the BFO-TAM station pair, for instance), which could reflect

(i) the intermittency of the excitation of the Gulf of Guinea source in 2004 August, (ii) possible other signals, occurring in the same period range, which outshine the redundant source phase arrival at some stations and/or (iii) multipathing effects.

Concerning the BFO-TAM station pair, the overall coherence maximum (which signs the phase redundancy) is observed at time lags corresponding approximately to the interstation great-circle surface wave propagation time, which is due to the position of the source almost aligned by chance on the great-circle path defined by the two stations. Such arrivals may typically alter tomography results based on empirical Green's function reconstruction from ambient noise cross-correlations (Shapiro & Campillo 2004). For all other station pairs, the emergence of the empirical Green's function is barely visible. Therefore, phase coherence statistics could be used to discriminate between different source contributions and thus may help to reduce potential traveltime biases due to persistent sources.

4 CONCLUSIONS

We present a new approach based on instantaneous phase coherence statistics to define the state of phase randomness for a set of synchronous signals. Both theory and synthetic experiment show that, in the fully random case, the mean and the variance of all possible pairwise comparisons equal to 0 and $\sqrt{1-2/\pi}$ ($\simeq$0.603), respectively. Any deviation from these values indicate the presence of a redundant phase. Using the ergodicity property of a random signal, we split an initial time-series into a set of synchronous signals. This allows to detect and to quantify the repetitiveness of any possible temporally persistent and spatially localized source, during a given period of observation.

In the case of the detection of a redundant phase, individual coherences (one trace against all others) quantify the contribution of each time-series independently. Depending on the application, the method may be used to exclude either poorly contributing traces for efficient signal extraction, or to exclude highly contributing traces to avoid contamination from a persistent signal. This method can be easily implemented to bring quantitative information on the ambient seismic wavefield.

ACKNOWLEDGEMENTS

This works is funded by the VIBRIS project (Council of Pays de la Loire, France). EB thanks CNRS-INSU 2014-SYSTER. MS thanks MISTERIOS (CGL2013-48601-C2-1-R). Data are provided by IRIS/IDA (doi:10.7914/SN/II) and GEOSCOPE. We acknowledge the editors J. Renner, M. Denolle, and an anonymous reviewer for the constructive comments.

REFERENCES

Bensen, G.D., Ritzwoller, M.H., Barmin, M.P., Levshin, A.L., Lin, F., Moschetti, M.P., Shapiro, N.M. & Yang, Y., 2007. Processing seismic ambient noise data to obtain reliable broad-band surface wave dispersion measurements, *Geophys. J. Int.,* **169**(3), 1239–1260.

Brenguier, F., Campillo, M., Hadziioannou, C., Shapiro, N., Nadeau, R. & Larose, E., 2008. Postseismic relaxation along the San Andreas Fault at Parkfield from continuous seismological observations, *Science,* **321,** 1478–1481.

Brzak, K., Gu, Y.J., Ökeler, A., Steckler, M. & Lerner-Lam, A., 2009. Migration imaging and forward modeling of microseismic noise sources near Southern Italy, *Geochem. Geophys. Geosyst.,* **10**(1), Q01012, doi:10.1029/2008GC002234.

Campillo, M., 2006. Phase and correlation in 'random' seismic fields and the reconstruction of the Green's function, *Pure appl. Geophys.,* **163**(2–3), 475–502.

Ebeling, C.W., 2012. Chapter one—Inferring ocean storm characteristics from ambient seismic noise: a historical perspective, in *Advances in Geophysics,* vol. 53, pp. 1–33, ed. Dmowska, R., Elsevier.

Gabor, D., 1946. Theory of communication, *J. IEE,* **93**(26), 429–457.

Gerstoft, P., Shearer, P.M., Harmon, N. & Zhang, J., 2008. Global P, PP, and PKP wave microseisms observed from distant storms, *Geophys. Res. Lett.,* **35**(23), L23306, doi:10.1029/2008GL036111.

Groos, J., Bussat, S. & Ritter, J., 2012. Performance of different processing schemes in seismic noise cross-correlations, *Geophys. J. Int.,* **188**(2), 498–512.

Holcomb, L.G., 1980. Microseisms: a twenty-six-second spectral line in long-period earth motion, *Bull. seism. Soc. Am.,* **70**(4), 1055–1070.

Kobayashi, N. & Nishida, K., 1998. Continuous excitation of planetary free oscillations by atmospheric disturbances, *Nature,* **395,** 357–360.

Koper, K.D., Seats, K. & Benz, H., 2010. On the composition of earth's short-period seismic noise field, *Bull. seism. Soc. Am.,* **100**(2), 606–617.

Lobkis, O.I. & Weaver, R.L., 2001. On the emergence of the Green's function in the correlations of a diffuse field, *J. acoust. Soc. Am.,* **110,** 3011–3017.

Longuet-Higgins, M.S., 1950. A theory of the origin of microseisms, *Phil. Trans. R. Soc. Lond.,* **243**(857), 1–35.

Mormann, F., Lehnertz, K., David, P. & Elger, C.E., 2000. Mean phase coherence as a measure for phase synchronization and its application to the eeg of epilepsy patients, *Phys. D,* **144**(3–4), 358–369.

Oliver, J., 1962. A worldwide storm of microseisms with periods of about 27 seconds, *Bull. seism. Soc. Am.,* **52**(3), 507–517.

Rhie, J. & Romanowicz, B., 2004. Excitation of Earth's continuous free oscillations by atmosphere ocean seafloor coupling, *Nature,* **431,** 552–556.

Schimmel, M., 1999. Phase cross-correlations: design, comparisons, and applications, *Bull. seism. Soc. Am.,* **89**(5), 1366–1378.

Schimmel, M. & Paulssen, H., 1997. Noise reduction and detection of weak, coherent signals through phase-weighted stacks, *Geophys. J. Int.,* **130,** 497–505.

Shapiro, N.M. & Campillo, M., 2004. Emergence of broadband Rayleigh waves from correlations of the ambient seismic noise, *Geophys. Res. Lett.,* **31**(7), L07614, doi:10.1029/2004GL019491.

Shapiro, N.M., Campillo, M., Stehly, L. & Ritzwoller, M.H., 2005. High-resolution surface-wave tomography from ambient seismic noise, *Science,* **307**(5715), 1615–1618.

Shapiro, N.M., Ritzwoller, M.H. & Bensen, G.D., 2006. Source location of the 26 sec microseism from cross-correlations of ambient seismic noise, *Geophys. Res. Lett.,* **33**(18), L18310, doi:10.1029/2006GL027010.

Stehly, L., Campillo, M. & Shapiro, N.M., 2006. A study of the seismic noise from its long-range correlation properties, *J. geophys. Res.,* **111**(B10), B10306, doi:10.1029/2005JB004237.

Taner, M.T., Koehler, F. & Sheriff, R.E., 1979. Complex seismic trace analysis, *Geophysics,* **44**(6), 1041–1063.

Tian, Y. & Ritzwoller, M.H., 2015. Directionality of ambient noise on the juan de fuca plate: implications for source locations of the primary and secondary microseisms, *Geophys. J. Int.,* **201**(1), 429–443.

Tonegawa, T., Fukao, Y., Takahashi, T., Obana, K., Kodaira, S. & Kaneda, Y., 2015. Ambient seafloor noise excited by earthquakes in the Nankai subduction zone, *Nat. Commun.,* **6,** 6132, doi:10.1038/ncomms7132.

White, R.O., 1991. Properties of instantaneous seismic attributes, *Leading Edge Explor.,* **10**(7), 26–32.

Xia, Y., Ni, S. & Zeng, X., 2013. Twin enigmatic microseismic sources in the gulf of guinea observed on intercontinental seismic stations, *Geophys. J. Int.,* **194**(1), 362–366.

Zeng, X. & Ni, S., 2010. A persistent localized microseismic source near the Kyushu Island, Japan, *Geophys. Res. Lett.,* **37**(24), L24307, doi:10.1029/2010GL045774.